Neuron
Article

NLF-1 Delivers a Sodium Leak Channel to Regulate Neuronal Excitability and Modulate Rhythmic Locomotion

Lin Xie,[1,2,8] Shangbang Gao,[2,8] Salvador M. Alcaire,[1,2] Kyota Aoyagi,[3] Ying Wang,[2] Jennifer K. Griffin,[4] Igor Stagljar,[5,6] Shinya Nagamatsu,[3] and Mei Zhen[1,2,6,7,*]
[1]Institute of Medical Science, University of Toronto, ON M5S 1A8, Canada
[2]Samuel Lunenfeld Research Institute, Toronto, ON M5G 1X5, Canada
[3]Department of Biochemistry, Kyorin University School of Medicine, Tokyo 181-8611, Japan
[4]Tanz Centre for Research in Neurodegenerative Diseases, Toronto, ON M5S 3H2, Canada
[5]Donnelly Centre, Department of Biochemistry, University of Toronto, Ontario, M5S 3E1, Canada
[6]Department of Molecular Genetics, University of Toronto, ON M5S 1A8, Canada
[7]Department of Physiology, University of Toronto, ON M5S 1A8, Canada
[8]These authors contributed equally to this work
*Correspondence: zhen@lunenfeld.ca
http://dx.doi.org/10.1016/j.neuron.2013.01.018

SUMMARY

A cation channel NCA/UNC-79/UNC-80 affects neuronal activity. We report here the identification of a conserved endoplasmic reticulum protein NLF-1 (*N*CA *l*ocalization *f*actor-1) that regulates neuronal excitability and locomotion through the NCA channel. In *C. elegans*, the loss of either NLF-1 or NCA leads to a reduced sodium leak current, and a hyperpolarized resting membrane potential in premotor interneurons. This results in a decreased premotor interneuron activity that reduces the initiation and sustainability of rhythmic locomotion. NLF-1 promotes axonal localization of all NCA reporters. Its mouse homolog mNLF-1 functionally substitutes for NLF-1 in *C. elegans*, interacts with the mammalian sodium leak channel NALCN in vitro, and potentiates sodium leak currents in primary cortical neuron cultures. Taken together, an ER protein NLF-1 delivers a sodium leak channel to maintain neuronal excitability and potentiates a premotor interneuron network critical for *C. elegans* rhythmic locomotion.

INTRODUCTION

A neuron's ability to elicit and propagate electric signals is determined intrinsically by its membrane properties including the resting membrane potential (RMP) (Hille, 2001). Neuronal RMP is established by the sodium (Na^+)/potassium (K^+) pump and background K^+ channels (Nicholls et al., 2001) and maintained by a persistent Na^+ permeability (Crill, 1996; Hodgkin and Katz, 1949). NALCN, the pore-forming α subunit of a newly defined four domain ion channel, accounts for a fraction of the tetrodotoxin-resistant, gadolinium (Gd^{3+})-sensitive Na^+ leak that depolarizes RMP and potentiates action potential firing in mouse hippocampal neurons (Lu et al., 2007). While NALCN shares considerable sequence homology to voltage-gated Na^+ and Ca^{2+} channels, it bears key amino acid differences. Most notably, it has a reduced number of negatively charged amino acids in the voltage-sensing S4 transmembrane segments, and its ion selectivity motif also deviates from the classic Na^+ and Ca^{2+} filters (Catterall, 2000a, 2000b). In vivo, the neuronal NALCN channel contributes to the Na^+ leak current at rest, and is potentiated upon the activation of neurotensin and substance P receptors (Lu et al., 2009). In pancreatic β cell lines, NALCN's activity contributes to an inward Na^+ current coupled with the activation of M3 muscarinic receptors (Swayne et al., 2009).

In parallel, putative invertebrate NALCN homologs were discovered in *C. elegans* (Humphrey et al., 2007; Jospin et al., 2007; Yeh et al., 2008) and *Drosophila* (Lear et al., 2005; Nash et al., 2002) and recently in snail (Lu and Feng, 2011). Previously, we and others showed that two *C. elegans* NALCN homologs, NCA-1 and NCA-2, function redundantly to affect *C. elegans* locomotion (Jospin et al., 2007; Pierce-Shimomura et al., 2008; Yeh et al., 2008). Wild-type *C. elegans* travels on a culture plate through the continuous and rhythmic propagation of sinusoidal body bends (see Movie S1A available online). A simultaneous loss of both the NCA-1 and NCA-2 pore subunits, referred to as *nca(lf)* henceforth, results in fainting, a unique motor deficit characterized by periodic halting during movement (Movie S1C; described and quantified further below). On the other hand, gain-of-function mutations in NCA-1, referred to as *nca(gf)* henceforth, lead to exaggerated body bending termed coiling (Yeh et al., 2008).

The in vivo physiological properties of these invertebrate channels remain to be determined. However, genetic studies of the behavioral phenotypes of *C. elegans* (Humphrey et al., 2007; Jospin et al., 2007; Yeh et al., 2008) and *Drosophila* (Humphrey et al., 2007) have led to the identification of UNC-79 and UNC-80, two conserved auxiliary subunits of this new channel. Multiple auxiliary subunits of sequence-related cation channels, such as the voltage-gated calcium channels (VGCCs),

promote the stabilization and membrane localization of the channel, and/or modulate channel gating and kinetics (Catterall, 2000b; Simms and Zamponi, 2012). Despite bearing no sequence similarity to known cation channel auxiliary subunits, UNC-79 and UNC-80 exert similar effects on the expression and localization of the NCA channel (Jospin et al., 2007; Yeh et al., 2008), and mUNC-80 couples the NALCN channel conductivity with an intracellular signaling cascade (Lu et al., 2010). In *C. elegans*, the loss of either UNC-79 or UNC-80 suppresses and reverts the coiler phenotype exhibited by *nca(gf)* to that of fainters (Yeh et al., 2008). *unc-79* and *unc-80* mutants exhibit a fainter phenotype identical to that of *nca(lf)* mutants. The loss of either UNC-79 or UNC-80 causes a reduced localization of NCAs along the axon. UNC-79 and UNC-80 also localize along the axon, but only in the presence of NCAs, implicating their copresence in a channel complex (Jospin et al., 2007; Yeh et al., 2008). Indeed, mouse mUNC-79 and mUNC-80 coimmunoprecipitated with NALCN (Lu et al., 2010). Identifying genetic suppressors of *nca(gf)* therefore effectively reveals subunits or effectors of this new channel.

Through genetic suppressor screens for *nca(gf)*, we identified another recessive, loss-of-function suppressor, *nlf-1*, that rescues the coiler phenotype exhibited by *nca(gf)* animals. Below, we present molecular, biochemical, electrophysiological, calcium imaging and behavioral analyses on *nlf-1* and *nca* that demonstrate (1) NCA contributes to a Na^+ leak current in *C. elegans* neurons; (2) NLF-1 is an ER resident protein that specifically promotes axon delivery of the NCA Na^+ leak channel; (3) NCA/NLF-1-mediated Na^+ leak current maintains the RMP and potentiates the activity of premotor interneurons to sustain *C. elegans'* rhythmic locomotion; (4) a mouse homolog mNLF-1 is functionally conserved with NLF-1 in vivo, and physically interacts with the mammalian Na^+ leak channel NALCN in vitro.

RESULTS

nlf-1 Functions in the Same Genetic Pathway as *nca*

We isolated a recessive, loss-of-function mutation allele (*hp428*) of the *nlf-1* gene that suppresses the behavioral phenotypes of *nca(gf)* mutants. A deletion allele *tm3631* for *nlf-1* was subsequently generated by the National Bioresource Project. *nca(gf)* exhibit exaggerated body bends during movements, resulting in periodic coiling (Yeh et al., 2008). *nca(gf);nlf-1* mutants exhibit movements in normal body bends and do not coil (data not shown).

Our qualitative and quantitative behavioral analyses placed *nlf-1* in the same genetic pathway as the *nca* genes. The locomotion deficit of *nca(lf), unc-79* and *unc-80* null mutants, referred to as fainters henceforth, is unique. The hallmark feature of fainter is the frequent halting during an otherwise grossly normal motor pattern, led by a relaxation of its anterior region that prevents body bend initiation and propagation (Figure 1A, top panels, denoted by asterisks). Qualitatively, both null allele *nlf-1* mutants (see below) exhibit characteristic fainter movements with frequent, brief halting, accompanied by a relaxed anterior body posture unique for fainters (Figure 1A; Movie S1B). They do not exhibit additional phenotypes from *nca(lf)* (Movies S1A and S1B).

We can describe fainter's motor deficit by two quantifiable parameters generated by automated behavioral analyses: relative idle/active states (Figure 1D) and rhythmicity in the motor pattern (Figures 1B and 1C). For idle/active states, we quantify the percentage of time that animals move and pause. An instantaneous speed of the centroid movement equal to/higher and less than 1 pixel/second is defined as movement and pausing, respectively (Experimental Procedures; Kawano et al., 2011). On our standard culture plates, while wild-type (N2) animals seldom stayed idle, the frequent halting by *nca(lf)* fainters led to a significantly increased fraction of the idle state (Figure 1D). For rhythmicity, we quantify the curvature of the anterior region during crawling (Figure 1A, bottom panels, denoted by a black asterisk and dashed line). Wild-type animals generated continuous and rhythmic sinusoidal body bending that propagated either posteriorly or anteriorly (Figure 1A, lower panels; Pierce-Shimomura et al., 2008). *nca(lf)* fainters exhibited discontinuous bending patterns (Figure 1A, lower panels), reflected by a drastic reduction of the bending curvature in the anterior body (Figure 1B, denoted by arrow heads; Figure 3A) that resulted in a significant reduction in body bending frequency (Figure 1C).

Like *nca(lf)*, *nlf-1* mutants showed an increased propensity for idle state (Figure 1D), a significantly reduced anterior bending curvatures (Figure 1B), and a reduced frequency of body bending initiation (Figure 1C). Both alleles exhibited similar degree of motor deficits (Figures 1A–1D). In all parameters, *nlf-1* mutants consistently exhibited slightly less severe phenotypes than *nca(lf)* (Figures 1B–1D). Critically, *nlf-1;nca(lf)* animals phenocopied *nca(lf)* in all parameters (Figures 1B–1D), and showed no additional phenotype from *nca(lf)* (Movies S1C and S1D). Lastly, while the loss of either functionally redundant α-subunits NCA-1 and NCA-2 alone failed to significantly alter *C. elegans'* locomotion, *nca-1(lf);nlf-1* and *nca-2(lf);nlf-1* mutants are strong fainters undistinguishable from *nca(lf)* (data not shown). Therefore, *nlf-1* functions in the same genetic pathway as the *nca* genes.

nlf-1 Encodes a Neuronal Endoplasmic Reticulum (ER) Protein

We mapped and cloned *nlf-1* (Experimental Procedures; Figures S1A and S1B). *nlf-1* encodes a protein with putative and uncharacterized vertebrate homologs (Figure S1C). They share moderate sequence homology at the central region, which we named as the NLF domain (Figures S1C and S1D). There is a lack of primary sequence homology outside the NLF domain, but putative ER retention motifs (RXR) and a predicted transmembrane segment are present at the N and C terminus, respectively, in NLF-1 and its putative homologs (Figure 2A). The *nlf-1(hp428)* allele harbors a guanine (G) to adenosine (A) mutation that alters the 3′ splice junction of the first intron, and the altered splice junction results in a single base pair deletion in the *hp428* cDNA that leads to a frame-shift and a premature stop codon (Figures 2A and S1B). The *nlf-1(tm3631)* allele deletes the N terminus of the gene (Figures 2A and S1B). Both alleles behaved as genetic null (Experimental Procedures) and are complete loss-of-function alleles of NLF-1.

Similar to NCA-1 (Jospin et al., 2007; Yeh et al., 2008), NLF-1 is expressed specifically, but broadly in the *C. elegans* nervous

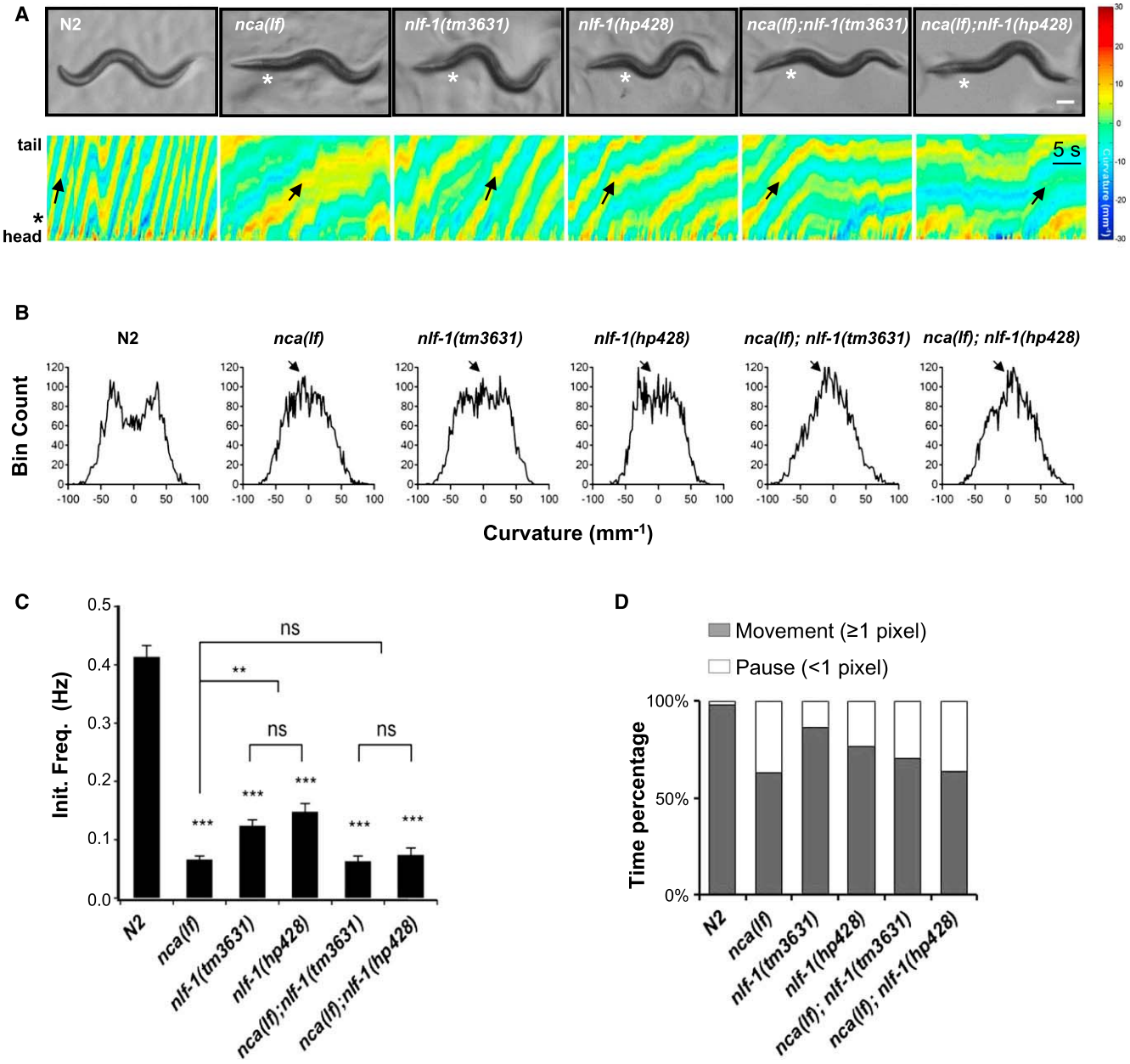

Figure 1. *nlf-1* Mutants Exhibit Hallmark Locomotion Deficits that Define Fainters

(A) Upper panel: snap shots of body postures of wild-type (N2), *nca(lf)*, *nlf-1(tm3631)*, *nlf-1(hp428)*, *nca(lf); nlf-1(tm3631)*, and *nca(lf); nlf-1(hp428)* animals on plates. White asterisks (*) denote the relaxed anterior region during pausing, a hallmark feature unique for fainters. *nlf-1(hp428)*, *nlf-1(tm3631)*, *nca(lf); nlf-1(tm3631)*, and *nca(lf); nlf-1(hp428)* phenocopied *nca(lf)*. Scale bar: 0.1 mm. Lower panel: body curvature matrices that describe *C. elegans'* sinusoidal movements. Color codes denote the body curvature from head to tail over 30 s. The propagating ventral and dorsal bending are presented as stripes of two color gradients. Fainters exhibited reduced frequency of body bends initiated from the anterior region and discontinuity during their propagation (arrow). Black asterisks (*) denote the anterior region where the curvature value was quantified (Figures 1B, 1C, 3B, and 6C) and plotted (Figure 3A).

(B) Anterior curvature value for animals of indicated genotypes. y axis refers to the total number of data points of a given curvature value from pooled images. *N2* exhibited two peaks at high curvature value representing ventral and dorsal bending. Fainters exhibit enrichment at low curvature value (arrows) that led to discontinuity in movements.

(C) The initiation frequency of anterior bending for animals of respective genotypes. Fainters exhibited a reduced bending frequency. Both alleles of *nlf-1* mutants showed slightly but statistically significantly higher frequency than that of *nca(lf)* and *nca(lf);nlf-1*.

(D) The overall activity states of animals of respective genotypes, quantified by percentages of time they spent in the pausing (white bars) or motion (gray bars) mode. A movement of the centroid <1 pixel/second (at 10×) is defined as pausing. All fainters exhibit a significantly increased propensity in pausing than N2 animals.

n = 865–1,918 frames (D), n = 10 animals (C). **p < 0.01; ***p < 0.001; ns, not significant by Student's t test. Error bars, SEM. See Figure S1 and Movie S1.

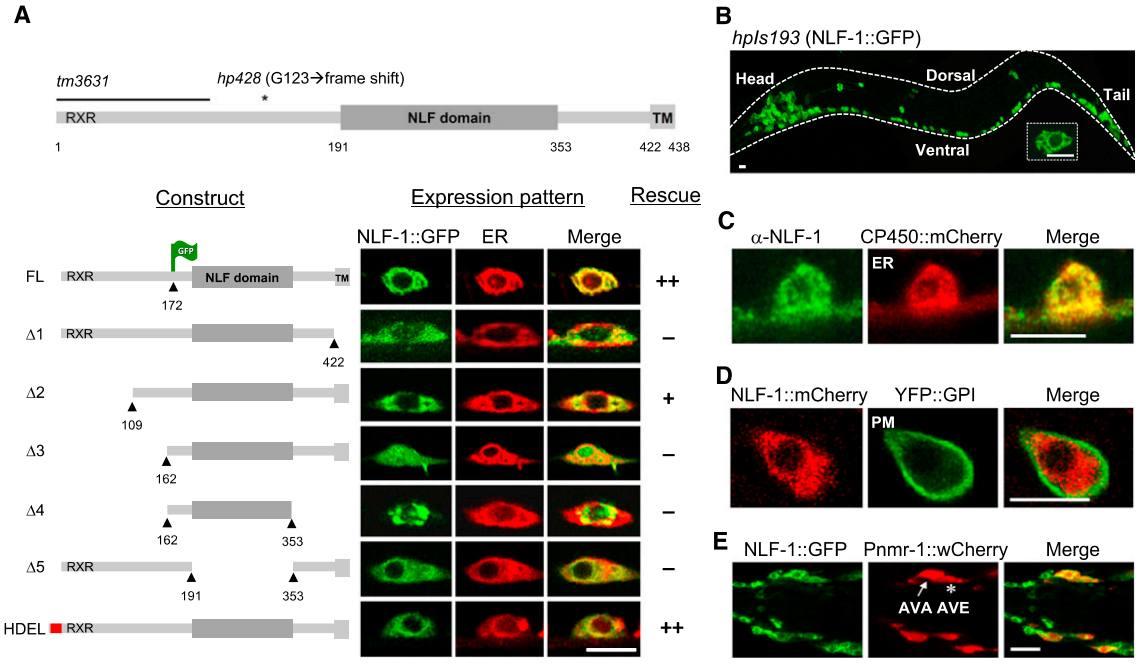

Figure 2. NLF-1 Is a Neuronal ER Protein

(A) Upper panel, predicted protein structure of NLF-1, and regions affected by the *tm3631* and *hp428* mutations. Lower panels, NLF-1::GFP deletion and ER-targeted constructs examined for their subcellular localization and function. ++ full rescue; + partial rescue; – no rescue of the *nlf-1(hp428)* locomotion defects.

(B) An adult *C. elegans* expressing functional *Pnlf-1*::NLF-1::GFP exhibited GFP signals in its nervous system, with an enlarged view of a single neuron. The animal is outlined by a dashed line.

(C) Confocal images of a wild-type ventral cord motor neuron coexpressing the *nlf-1* genomic fragment and an ER marker CP450::mCherry.

(D) Confocal images of a neuron coexpressing NLF-1::mCherry and or a plasma membrane marker YFP::GPI.

(E) Confocal images of an animal coexpressing *Pnlf-1*::NLF-1::GFP and a premotor interneuron marker *Pnmr-1*::wCherry.

Scale bars, 50 and 5 μm (A), 5 μm (C and D),10 μm (E). See Figure S2.

system (Figures 2B, 2E, S2G, and S2H). Consistent with the presence of putative ER retention signals in NLF-1, a fully functional NLF-1::GFP or NLF-1::FLAG, driven by its endogenous promoter, colocalized with multiple ER reporters (CP450::mCherry, mCherry::SP12 and mCherry::TRAM) in neurons (Figures 2C and S2A–S2C; data not shown). They did not colocalize with a plasma membrane (YFP::GPI; Figure 2D) or a Golgi (ManII::mCherry; Figure S2D) reporter. NLF-1::RFP from *C. elegans* lysates exhibited a mobility shift when treated with Endoglycosidase H (EndoH) (Figure S6D), which removes N-linked glycosylation from proteins in the ER or early Golgi apparatus, but not glycosylation in later stages of the secretory pathway (Helenius and Aebi, 2001; Grunwald and Kaplan, 2003). No EndoH-resistant fraction of NLF-1::RFP could be detected (Figure S6D), consistent with its ER-restricted localization.

The ER retention of NLF-1 fusion proteins was not caused by the GFP or FLAG tags. Although our NLF-1 antibodies (Experimental Procedures) were unable to detect the protein at an endogenous level, the immunofluorescent staining of a strain expressing a multi-copy array of an untagged *nlf-1* genomic fragment revealed an ER-restricted localization identical to that of NLF-1 fusion proteins (Figures 2C, S2A, and S2B). Structure-function analysis of NLF-1 demonstrated that both N- and C-terminal regions of NLF-1 were required for its ER-restricted localization (Figure 2A). Perturbing NLF-1's ER localization led to complete abolishment (Figure 2A, Δ1, Δ3, Δ4) or reduction (Figure 2A, Δ2) of its ability to restore the locomotion defect of *nlf-1* mutants (Figure S2E). By contrast, tagging NLF-1 with HDEL, a known ER-retention signal (Basham and Rose, 2001; Denecke et al., 1992; Semenza et al., 1990) did not alter its ER localization (Figure 2A, HDEL) or affect its rescuing ability (Figure S2F). Therefore, NLF-1's ER localization is critical for its function.

Collectively, these data indicate that NLF-1 is a novel ER resident protein that functions in the same biological process as the NCA channel.

NLF-1 Is Critically Required in Premotor Interneurons to Prevent Fainting

To determine the physiological deficit that underlies the fainting phenotype shared by *nlf-1* and *nca* mutants, we first identified the minimal neural network that contributes most critically to this movement deficit. While NLF-1 is expressed in sensory neurons, interneurons (Figure 2E) and excitatory motor neurons (Figure S2G), the restored expression of NLF-1 in the premotor interneurons, a subset of interneurons that input directly onto the motor neurons, was necessary to restore the initiation and continuity of rhythmic locomotion in *nlf-1* mutants (Figures 3A,

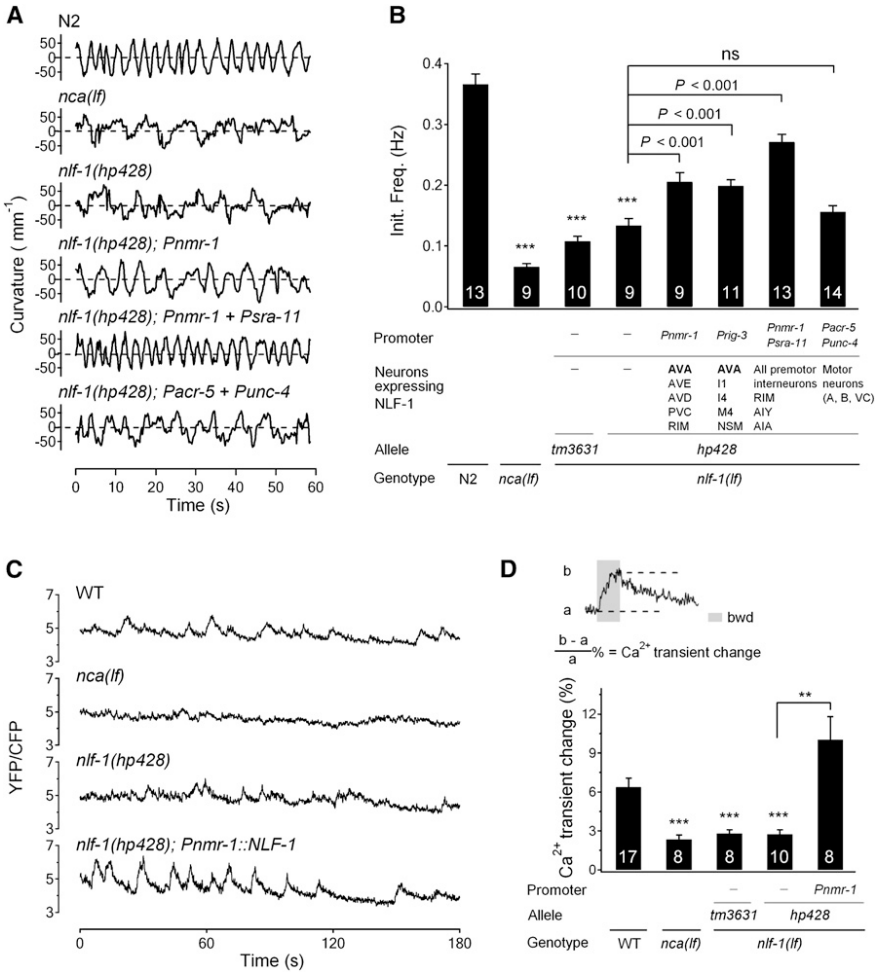

Figure 3. NLF-1 Is Critically Required in Premotor Interneurons to Regulate Locomotion

(A) Sample traces of spontaneous *C. elegans* movements, represented by the change of their anterior body curvature over time. N2 (wild-type) animals exhibit a rhythmic bending pattern. In *nca(lf)* and *nlf-1* mutants, they exhibited pauses between and during the bending cycle, which led to movement discontinuity, and a reduction of the initiation frequency of body bending. Restoring the expression of *nlf-1* in all premotor neurons (*Pnmr-1 + Psra-11*) significantly rescued the bending frequency defects in *nlf-1(hp428)* animals, whereas an expression of *nlf-1* in motor neurons (*Pacr-5 + Punc-4*) did not increase the frequency. Restoring NLF-1 in subgroups of premotor interneurons (AVA/AVE by *Pnmr-1*) was sufficient for a partial, similar rescue of bending frequency.

(B) Quantification of the body bending initiation frequency. NLF-1 expression in premotor neurons (*Pnmr-1*, *Prig-3*) but not in motor neurons (*Pacr-5*, *Punc-4*), was necessary for increasing the bending frequency for *nlf-1* mutants. n = 8–15 animals.

(C) Representative calcium transients in coimaged AVA/AVE indicated by the YFP/CFP ratio of a cameleon reporter in N2 (WT) and fainter animals over time.

(D) Top panel, a representative calcium transient change, overlaid with the animal's movement (gray area indicates backing). Lower panel, change in the mean AVA/AVE calcium transient during backing was reduced in fainters. n = 8–17 animals. ns, not significant.

**p < 0.01, ***p < 0.001, against reference wild-type (N2 in B; WT in D by the Mann-Whitney U test). Error bars, SEM. See Figure S3 and Movie S1.

3B, and S3B; *Pnmr-1+Psra-11*), and to prevent frequent halting (Figure S3A; *Pnmr-1+Psra-11*). By contrast, restoring the NLF-1 expression in motor neurons did not rescue fainting (Figures 3A, 3B, S3A, and S3B; *Pacr-5+Punc-4*). Similarly, the locomotion defect of *unc-79* fainters was only rescued by restoring their expression in premotor interneurons, not in motor neurons (data not shown). These results point to dysfunctional premotor interneurons, rather than a lack of motor activity, being the primary cause of the failure in the initiation and maintenance of rhythmic locomotion exhibited by fainters.

Among all premotor interneurons, restoring NLF-1 expression in a subgroup, including AVA and AVE, led to the most significant, partial rescue of fainting (Figures 3A, 3B, and S3B; *Pnmr-1*). Through real-time calcium imaging, we recently demonstrated that the AVA and AVE premotor interneurons exhibit similar activity profiles during spontaneous movements (Kawano et al., 2011). In wild-type animals, coimaged AVA and AVE exhibited large and periodic rise in intracellular Ca^{2+} that temporally correlated with the initiation and duration of backing (Kawano et al., 2011; Figures 3C and 3D). In both *nca(lf)* and *nlf-1* mutants, pulses of Ca^{2+} transients in AVA and AVE exhibited a significantly reduced amplitude (Figures 3C and 3D), which corresponded with shorter backing, and indicates a reduced premotor interneuron activity. Restoring NLF-1 expression only in these neurons fully restored the Ca^{2+} transient profile (Figures 3C and 3D). These transgenic animals exhibited Ca^{2+} transients that were slightly higher than wild-type animals (Figure 3D), which may be caused by NLF-1 overexpression. These results imply that NLF-1 and the NCA channel potentiate premotor interneurons, whose activity is most critical to maintain the continuity of locomotion.

NLF-1 and NCA Contribute to a Na^+ Leak Current that Maintains the RMP of Premotor Interneurons

To pinpoint the physiological origin of a reduced premotor interneuron activity in *nlf-1* and *nca(lf)* mutants observed by calcium imaging, we examined the membrane properties of the AVA premotor interneuron by in situ whole-cell recording using a dissected *C. elegans* preparation (Kawano et al., 2011).

First, we identified a Na^+ leak current in AVA that depends, in part, on NLF-1 and NCA (Figures 4A–4C and 4G). In wild-type animals, this leak conductance was voltage-independent (Figures S4A and S4B), regulated by extracellular Na^+ (Figures 4A–4C), and was partially and reversibly blocked by Gd^{3+} across potentials (Figures S4A–S4E). In both *nlf-1* and *nca(lf)* mutants, this Na^+ leak current was significantly reduced (Figures 4A, 4B,

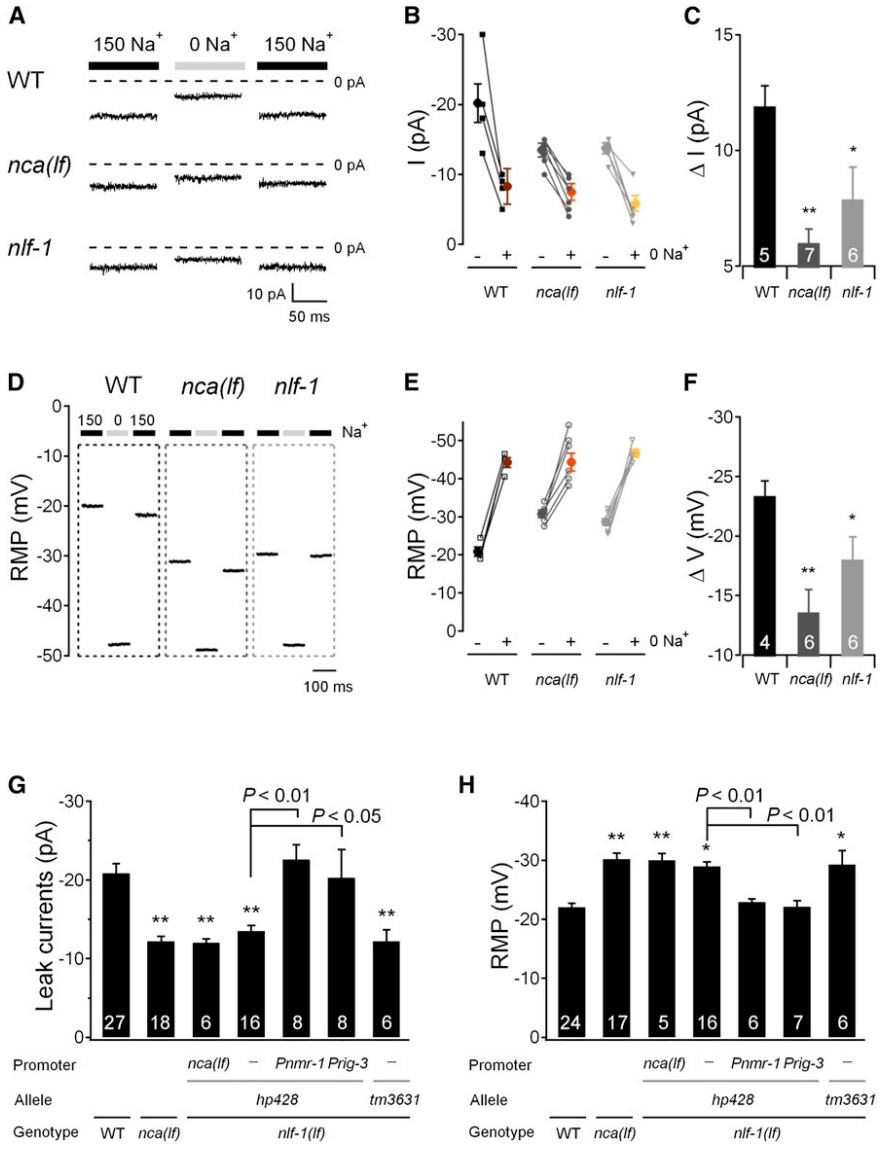

Figure 4. NLF-1 and NCA Mediate a Na^+ Leak Current that Maintains the RMP of AVA

(A) Representative traces of AVA leak currents (at −60 mV) in the presence (150 mM Na^+), absence (0 Na^+), and wash back (150 mM Na^+) of extracellular sodium ($[Na^+]_o$), with 5–20 s interval between solution changes.

(B) Leak currents before and after the removal of $[Na^+]_o$. Connected lines represent recordings from the same neuron.

(C) Quantified leak current changes upon the removal of $[Na^+]_o$ in wild-type, *nca(lf)*, and *nlf-1* mutants.

(D–F) Representative traces and quantification of AVA RMP in the presence and absence of $[Na^+]_o$ in wild-type, *nca(lf)*, and *nlf-1* mutants.

(G and H), Both reduced Na^+ leak currents and hyperpolarized RMP in AVA were fully rescued when NLF-1 expression was restored in AVA of *nlf-1(hp428)*.

*p < 0.05; **p < 0.01; Student's t test against wild-type. Error bars, SEM. See Figure S4.

4G, and S4A). Gd^{3+} failed to block the residual Na^+ leak currents in either mutant (Figures S4C–S4E). These results imply that NLF-1 and the NCA channel account for the Gd^{3+}-sensitive Na^+ leak current. The reduced Na^+ leak current in AVA in *nlf-1* mutants was fully rescued by restoring NLF-1 expression in AVA (Figure 4G; *Pnmr-1*, *Prig-3*).

The NLF-1/NCA-mediated Na^+ leak current is critical for the maintenance of neuronal RMP. In both *nlf-1* and *nca(lf)* mutants, AVA became hyperpolarized (∼−30 mV versus ∼−20 mV in wild-type animals; Figures 4D and 4H). This defect was fully rescued when NLF-1 was restored in AVA of *nlf-1* mutants (Figure 4H; *Pnmr-1, Prig-3*). AVA RMP depended on extracellular Na^+. In wild-type, *nlf-1* and *nca(lf)* animals, removal of extracellular Na^+ all led to a hyperpolarization of AVA (Figures 4D–4F). The decrease, however, was significantly less in *nlf-1* and *nca(lf)* (Figures 4E and 4F). Moreover, consistent with NCA and NLF-1 constituting the Gd^{3+}-sensitive sodium leak currents, Gd^{3+} led to prominent AVA hyperpolarization in wild-type animals (Figures S4F–S4H), but not in *nlf-1* and *nca(lf)* mutants (Figures S4F–S4G). Lastly, *nlf-1;nca(lf)* double mutants did not exhibit a further decrease in either the Na^+ leak current, or the RMP of AVA, from *nlf-1* or *nca(lf)* (Figures 4G and 4H; *nca(lf)* in the *nlf-1(lf)* subsection).

Taken together, NLF-1 contributes to an NCA channel-mediated Na^+ leak current that maintains the RMP, hence the excitability and activity of *C. elegans* premotor interneurons.

NLF-1 Promotes the Axonal Localization of the NCA Channel

How does an ER protein regulate neuronal excitability? Channels are synthesized and assembled at the ER prior to their delivery to the plasma membrane (Deutsch, 2003). We investigated a hypothesis that NLF-1 is an ER resident protein specifically required for the folding, assembly, and delivery of the NCA Na^+ leak channel by examining the localization of its known subunits.

In *nlf-1* mutants, all known NCA channel subunits, functional NCA-1::GFP (Figure 5A), NCA-2::GFP (Figure 5A), UNC-79::GFP (Figure S5A), and UNC-80::RFP reporters (Figure S5B), exhibited a drastic reduction in axon membrane localization. Weak NCA-1::GFP and NCA-2::GFP signals were observed at the ER of neural soma in *nlf-1* mutants, but also in wild-type animals, likely due to an overexpression of the transgene reporters (not shown). Endogenous UNC-79 level was significantly, and partially decreased in *nlf-1* mutants (Figure 5B). In adult *nlf-1* mutants, a short pulse of NLF-1 expression driven by a heat-shock promoter (Experimental Procedures) was

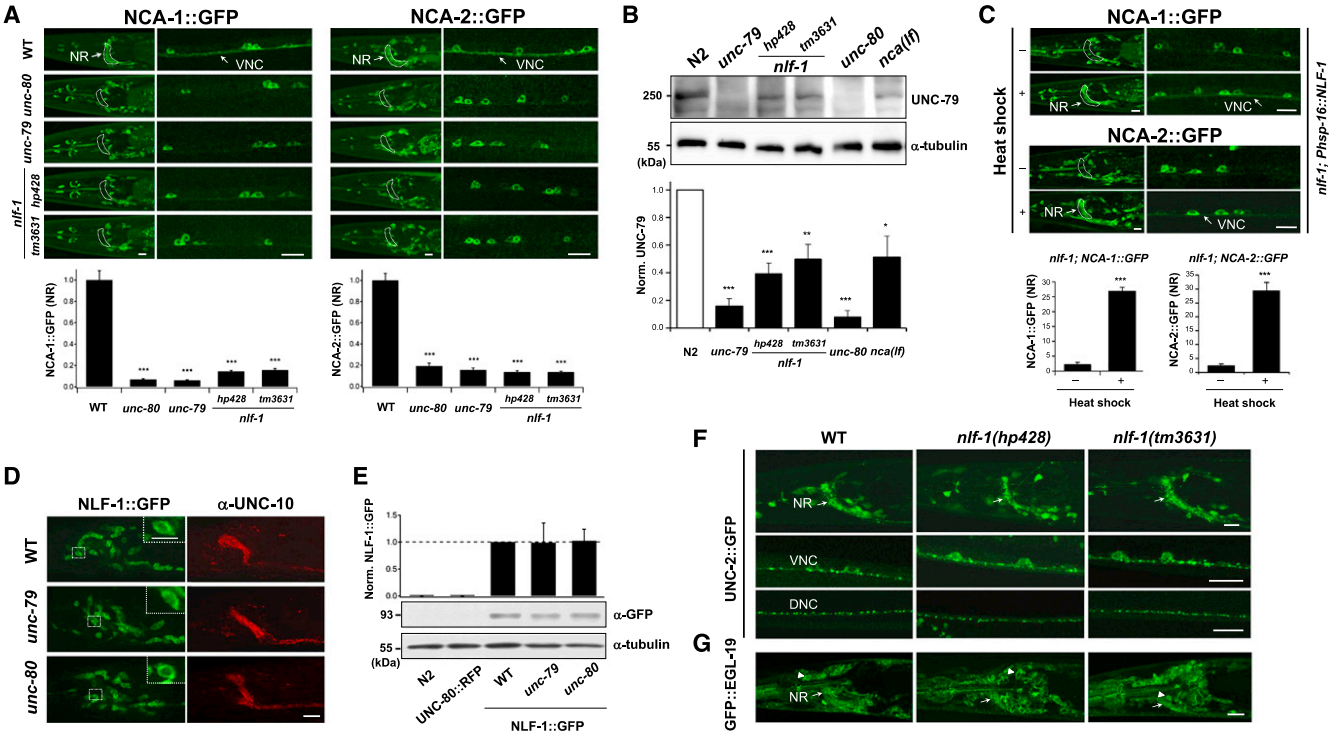

Figure 5. NLF-1 Facilitates Axon Localization of the NCA Channel

(A) Representative confocal images (upper panels) and quantification (lower panel) of a functional NCA-1::GFP and NCA-2::GFP transgene (WT) of various genotypes. NCAs::GFP signals in axons of sensory and interneurons (left, NR, arrows) and of motor neuron processes (right, VNC, arrows), but not in the soma, were decreased in all mutants. n = 8–10 for NCA-1::GFP; n = 5–9 for NCA-2::GFP.

(B) Endogenous UNC-79 level in *N2*, *unc-79*, *nlf-1(hp428)*, *nlf-1(tm3631)*, *unc-80*, and *nca(lf)* animals. UNC-79 was partially but significantly decreased in both *nlf-1* mutants.

(C) Acute NLF-1 expression restores axon localization of the NCA-1::GFP and NCA-2::GFP reporters.

(D) The ER localization NLF-1::GFP were unaltered by the absence of NCA channel components. Animals were coimmunostained with anti-GFP (for NLF-1, green) and anti-UNC-10 (for axons, red). WT, an integrated functional NLF-1::GFP transgene. *unc-79* and *unc-80* mutants carry the same transgene.

(E) NLF-1::GFP level was not altered in fainter mutants. Total protein lysates from nontransgenic (N2) and UNC-80::RFP animals served as controls for anti-GFP antibodies. n = 5.

(F) Confocal images of a functional P/Q/N-type VGCC/UNC-2::GFP reporter. Punctate UNC-2::GFP signals were present at axons of the sensory and interneurons (NR, arrows) and motor neurons (VNC, DNC) in both wild-type (left panels) and *nlf-1* (middle and right panels) animals.

(G) Confocal images of a functional L-type VGCC GFP::EGL-19 reporter. GFP signals were observed mostly in neuron soma (arrowhead) and weakly in axons (NR) in both wild-type and *nlf-1* mutants.

n.s., not significant; *p < 0.05, **p < 0.01, ***p < 0.001 against WT by Mann-Whitney U test. Error bars, SEM. Scale bars, 10 μm. See Figure S5.

sufficient to restore the axonal localization of NCA-1::GFP and NCA-2::GFP (Figure 5C), as well as the fainting behavior (not shown). An acute rescue of *nlf-1* mutants supports a direct role of NLF-1 in promoting rapid assembly and/or delivery of functional NCA channels to axons.

Supporting the notion that NLF-1 functions specifically with the NCA Na^+ leak channel, the axon and/or soma localization and abundance of two sequence-related VGCC reporters, the P/Q/N-type UNC-2::GFP (Saheki and Bargmann, 2009) and L-type GFP::EGL-19 (Arellano-Carbajal et al., 2011), were unaffected in *nlf-1* mutants (Figures 5F and 5G). *nlf-1* mutations did not suppress the locomotion defects exhibited by either *unc-2(gf)* (S.M.A. and M.Z., unpublished data) or *egl-19(gf)* (Lee et al., 1997) animals (not shown).

The ER localization and abundance of NLF-1::GFP was unaffected by the absence of NCA channel components UNC-79 and UNC-80 (Figures 5D and 5E). We could not examine NLF-1 expression in *nca(lf)* mutants because the NLF-1::GFP transgene was integrated closely to the *nca-1* locus. Collectively, these results indicate that NLF-1 is an ER protein that specifically promotes the axonal localization of the NCA channel.

A Mouse Homolog mNLF-1 Is Functionally Conserved

The sequence homology between NLF-1 and its putative vertebrate homologs is restricted and overall fairly modest, raising concerns for their physiological relevance. Two predicted mouse genes exhibit sequence homology to *nlf-1*. We isolated cDNA for one such homolog, mNLF-1, from the mouse brain (Experimental Procedures and Supplemental Information). Driven by a *C. elegans* panneural promoter, the expression of either mNLF-1, or mNLF-1::GFP in *nlf-1* mutants fully rescued their fainting behavior (Figures 6A–6C). Despite lacking primary sequence homology outside the NLF domain, the functional mNLF-1::GFP also exhibited ER-restricted localization

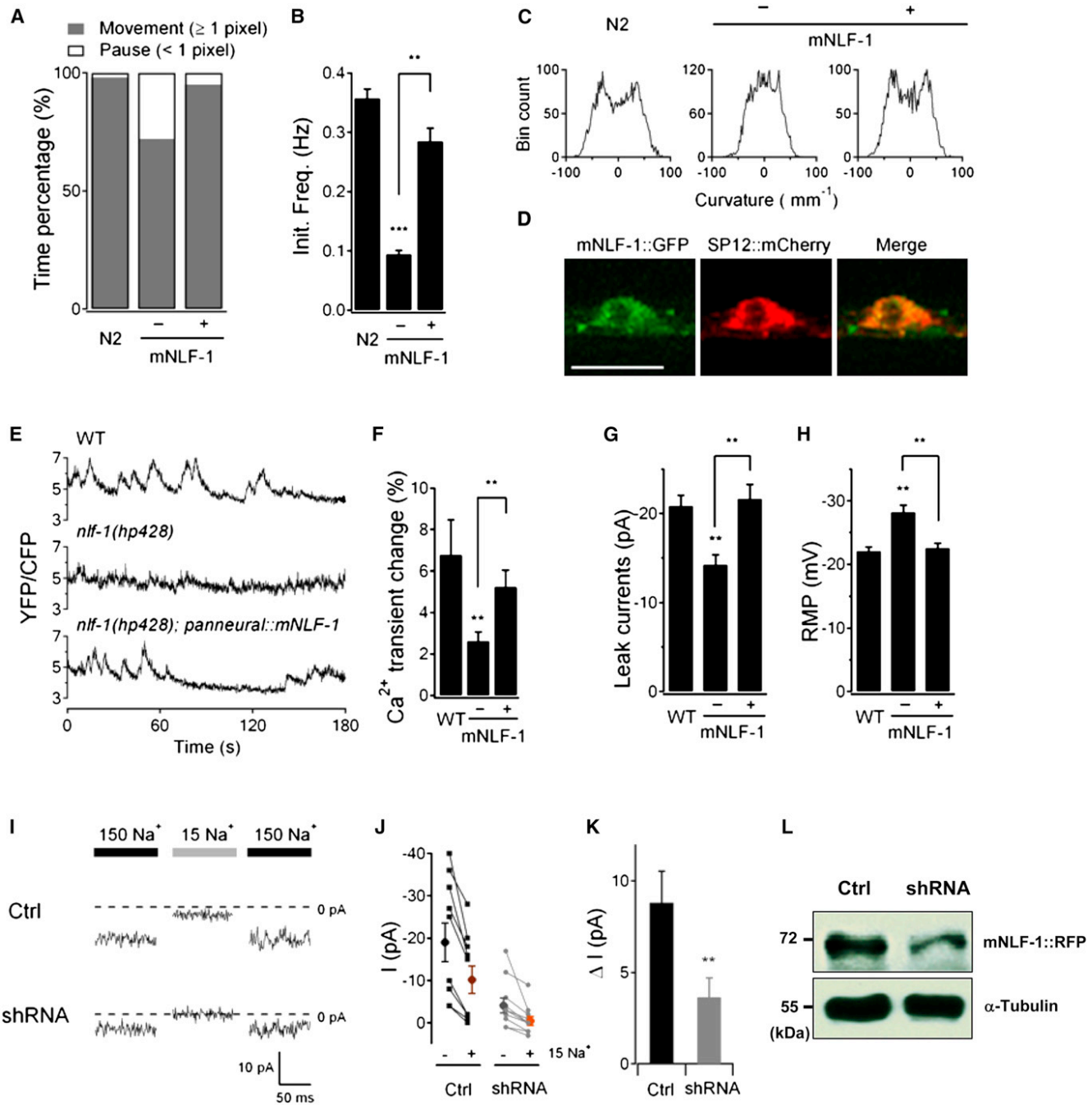

Figure 6. mNLF-1 Is Functionally Conserved with NLF-1

(A–C) A panneuronal (*Prgef-1*) expression of mNLF-1 in *nlf-1(hp428)* mutants fully restored their locomotion deficits—the increased overall activity states (A), restored initiation frequency of body bending (B), and an increased overall anterior body curvature (C). n = 900–1,085 frames (A), n = 10–11 animals (B and C).

(D) A functional, panneuronally expressed mNLF-1::GFP was localized to the ER of *C. elegans* neurons. Scale bar, 10 μm.

(E) Representative calcium profiles of coimaged AVA/AVE in respective genotypes.

(F) A panneuronally expressed mNLF-1 fully restored the peak calcium transient rise in *nlf-1(hp428)* mutants. n = 10–14 animals.

(G and H) A panneuronally expressed mNLF-1 fully rescued the decreased Na^+ leak currents (G) and hyperpolarized RMP (H) of the AVA premotor interneuron in *nlf-1(hp428)* mutants. n ≥ 7 animals.

(I) Representative leak current traces (holding at −85 mV) of mouse cortical neurons transfected with scrambled (Ctrl), or shRNA against mNLF-1.

(J) Leak currents before and after the decrease of $[Na^+]_o$. Connected lines represent recordings from the same neuron.

(K) Quantified leak current changes upon the reduction of $[Na^+]_o$, n ≥ 10 cells.

(L) Western blot analyses of primary cortical neuron cultures where mNLF-1::RFP was cotransfected with either scrambled (Ctrl) or mNLF-1 shRNA constructs.

Error bars, SEM. *p < 0.05, **p < 0.01, ***p < 0.001 by the Mann-Whitney U test or Student's t test. See Figure S6.

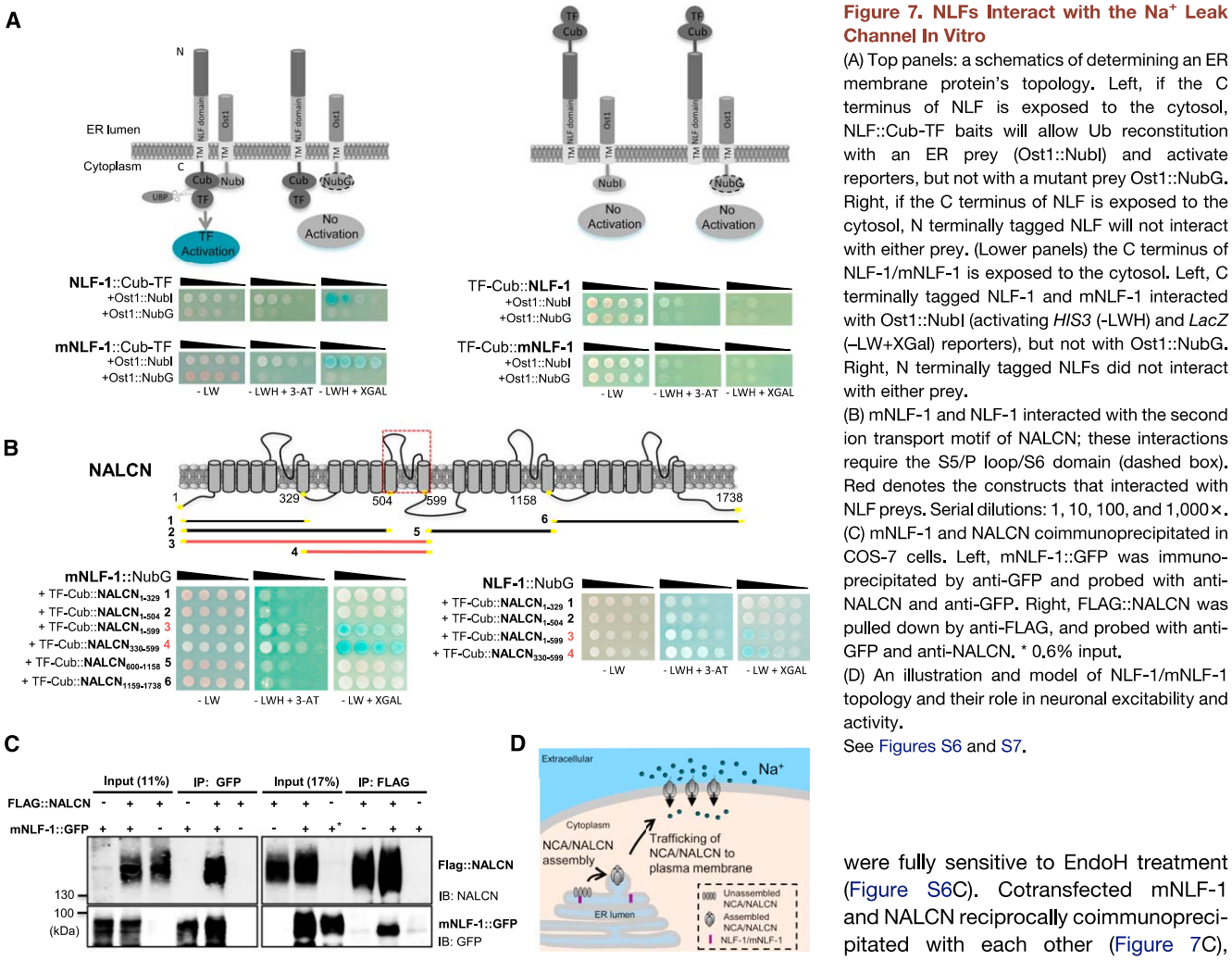

Figure 7. NLFs Interact with the Na^+ Leak Channel In Vitro

(A) Top panels: a schematics of determining an ER membrane protein's topology. Left, if the C terminus of NLF is exposed to the cytosol, NLF::Cub-TF baits will allow Ub reconstitution with an ER prey (Ost1::NubI) and activate reporters, but not with a mutant prey Ost1::NubG. Right, if the C terminus of NLF is exposed to the cytosol, N terminally tagged NLF will not interact with either prey. (Lower panels) the C terminus of NLF-1/mNLF-1 is exposed to the cytosol. Left, C terminally tagged NLF-1 and mNLF-1 interacted with Ost1::NubI (activating *HIS3* (-LWH) and *LacZ* (–LW+XGal) reporters), but not with Ost1::NubG. Right, N terminally tagged NLFs did not interact with either prey.

(B) mNLF-1 and NLF-1 interacted with the second ion transport motif of NALCN; these interactions require the S5/P loop/S6 domain (dashed box). Red denotes the constructs that interacted with NLF preys. Serial dilutions: 1, 10, 100, and 1,000×.

(C) mNLF-1 and NALCN coimmunoprecipitated in COS-7 cells. Left, mNLF-1::GFP was immunoprecipitated by anti-GFP and probed with anti-NALCN and anti-GFP. Right, FLAG::NALCN was pulled down by anti-FLAG, and probed with anti-GFP and anti-NALCN. * 0.6% input.

(D) An illustration and model of NLF-1/mNLF-1 topology and their role in neuronal excitability and activity.

See Figures S6 and S7.

(Figure 6D), identical to that of NLF-1 and NLF-1::GFP in *C. elegans* neurons. The panneuronally expressed mNLF-1 fully restored AVA/AVE premotor interneuron's activity in *nlf-1* mutants by calcium imaging analyses (Figures 6E and 6F). Critically, this rescue coincided with an increased Na^+ leak current (Figure 6G) and a restored RMP (Figure 6H) in the AVA premotor interneurons. Therefore, mNLF-1 can functionally substitute for NLF-1 in *C. elegans* neurons. Lastly, in primary mouse cortical neuron cultures, shRNA against mNLF-1 effectively and partially reduced the background Na^+ leak currents (Figures 6I–6L), further supporting the functional conservation of the NLF proteins. Both results highlight a remarkable structural and functional conservation of this Na^+ leak channel complex.

mNLF-1 Interacts with NALCN In Vitro

If NLF proteins participate specifically in the folding, assembly or delivery of the Na^+ leak channel, they may transiently interact at the ER. We first examined this possibility in transfected mammalian cells. Similar to the case in *C. elegans* neurons, mNLF-1::GFP or mNLF-1::RFP exhibited ER-restricted localization in transfected mammalian cells (Figures S6A and S6B), and were fully sensitive to EndoH treatment (Figure S6C). Cotransfected mNLF-1 and NALCN reciprocally coimmunoprecipitated with each other (Figure 7C), whereas cotransfected mNLF-1 and mUNC-80 did not (Figure S6E). Supporting a role of mNLF-1 in the stabilization of the NALCN channel, the NALCN level was significantly increased when co-expressed with mNLF-1 (Figures S6F and S6G).

We further employed a membrane yeast two-hybrid (MYTH) assay to determine their membrane topology (Deribe et al., 2009; Gisler et al., 2008; Johnsson and Vershavsky, 1994). Briefly, this system takes advantage of the ability of ubiquitin to functionally reconstitute from two split C- and N-terminal ubiquitin (Ub) fragments, Cub and NubI. When a transcription factor (TF) is tagged to Cub, upon Ub reconstitution, TF is released by ubiquitin-specific proteases (UBPs) and activates reporters. When Cub-TF and NubI are tagged to membrane proteins, both tags must be exposed to the cytosol to enable Ub reconstitution and reporter activation (Figure 7A, illustration). NubG harbors a mutation that prevents auto-reconstitution with Cub, but allows Ub reconstitution when they are brought into proximity by proteins they are tagged to.

To examine whether mNLF-1/NLF-1 reside at the ER in yeast, and if so, their membrane topology, mNLF-1 and NLF-1 were tagged with Cub-TF at either the N- (TF-Cub::NLF) or C- (NLF::Cub-TF) terminal. They were tested for interactions

with Ost1::NubI, a yeast ER integral membrane prey with its Nub tag exposed to the cytosol. If NLFs are not membrane anchored, but cytoplasmic proteins, both N and C terminally tagged baits will interact with the prey. If they are membrane anchored, the prey will selectively interact with either N or C terminally tagged construct that exposes Cub-TF to the cytosol. Only C terminally tagged NLF-1 and mNLF-1 interacted with Ost1::NubI (Figure 7A, left panels), indicating that their N terminus reside in the ER. They did not interact with Ost1::NubG, the control prey that prevents Ub auto-reconstitution (Figure 7A, left panels). N terminally tagged NLF baits did not interact with either Ost1::NubI or Ost1::NubG (Figure 7A, right panels), confirming the membrane anchoring of both baits. Therefore, both NLF-1 and mNLF-1 exhibit a tail-anchored, type I ER membrane topology.

The topology of NLF allows mapping interactive motifs with channel components. A C terminally tagged NLF::NubG prey exposed the tag to the cytosol, but rendered Ub reconstitution strictly dependent on NLF's interaction with the bait. Among multiple baits comprised of different segments of NALCN that were properly oriented in the membrane (Figure S7A), both mNLF-1 and NLF-1 interacted robustly, and specifically with NALCN's second ion transport motif (Figure 7B, constructs 3 and 4). These interactions required its S5/P loop/S6 segment (Figure 7B, compare constructs 2 and 3). Replacing this segment with an analogous region of a P/Q/N-type VGCC UNC-2, or a L-type VGCC EGL-19 also abolished the interaction (Figures S7B and S7C). Other NALCN channel components (mUNC-79 and mUNC-80), and an innexin channel (UNC-7), did not exhibit interactions with NLFs (not shown).

DISCUSSION

Our molecular genetic, biochemical and physiological analyses uncover NLF-1/mNLF-1, a conserved ER regulator of a Na^+ leak channel NCA/NALCN, which maintains the RMP and activity of a small premotor interneuron network responsible for the maintenance of *C. elegans'* rhythmic locomotion (Figure 7D).

NLF-1 Functions Specifically with the NCA Na^+ Leak Channel

Our current data suggest a remarkable functional specificity of NLF-1 with a Na^+ leak channel NCA. *nlf-1* mutants exhibit behavioral phenotypes unique and characteristic of the loss-of-function mutants for the NCA channel components, with no additional phenotypes from *nca(lf)*. *nlf-1* null alleles do not enhance *nca(lf)* defects in locomotion or in AVA membrane properties. Other *C. elegans* cation channel mutants, while uncoordinated in locomotion, do not faint. *nlf-1* suppresses the *nca(gf)* movement pattern but does not suppress that of *VGCC(gf)* mutants. Genetically, these results place *nlf-1* fairly specifically in the biological pathway as the *nca* genes. Consistently, all NCA channel component reporters, despite being overexpressed, exhibit drastic reduction of axonal localization in the absence of NLF-1. On the other hand, sequence-related VGCC reporters are unaffected in *nlf-1* mutants, although a subtle difference of endogenous level could be masked by reporter overexpression.

NLF-1 Functions as an ER Regulator for the Na^+ Leak Channel

NLF-1 may achieve its functional specificity as an auxiliary subunit unique for the Na^+ leak channel. Multiple lines of evidence, however, suggest NLF-1's role at the ER. NLF-1, as well as ectopically expressed mNLF-1, are restricted at the ER of *C. elegans* neurons. mNLF-1 also localizes to the ER in yeast and mammalian cells. Importantly, disrupting NLF-1's ER localization diminishes, or severely reduces its rescuing ability of *nlf-1* mutants.

Although many ER proteins are promiscuous facilitators for the folding and delivery of membrane proteins, ER resident proteins with remarkable substrate and functional specificity, such as RIC-3 that facilitates the surface expression of subtype nicotinic acetylcholine receptors (Halevi et al., 2002; Lansdell et al., 2005), CALF-1 that affects axon localization of the *C. elegans* P/Q/N-type VGCC UNC-2 (Saheki and Bargmann, 2009), and SARAF that interacts with STIM1 to regulate store-operated calcium entry (Palty et al., 2012), are present. NLF-1 may represent another example of an emerging class of ER proteins with substrate specificity.

At the ER, NLF-1/mNLF-1 may function as chaperones to facilitate the folding and assembly of the Na^+ leak channel subunit. A failure in folding and assembly could result in membrane proteins being targeted for degradation instead of trafficking (Altier et al., 2011; Gong et al., 2005; Waithe et al., 2011). Indeed, in *nlf-1* mutants, all NCA channel reporters exhibit drastic reduction of axonal localization. This coincides with a reduced level of an endogenous channel component in *C. elegans nlf-1* mutants, as well as an increase of the NALCN level when cotransfected with mNLF-1 in mammalian cells. Upon folding, NLFs may further facilitate their ER exit, either by masking ER-retention motifs, or coupling them with exit machineries such as COPII coats.

Deciphering precise mechanisms through which NLF-1/mNLF-1 promote the sodium leak channel's axon localization requires further investigation. Our current studies suggest an involvement of the physical interaction between NLFs and the pore subunit of the Na^+ leak channel. NLFs and the Na^+ leak channel interacted with each other in vitro. The removal, or replacement of the second S5/P loop/S6 motif of the channel with analogous motifs from two sequence-related VGCCs abolished interactions with NLFs. Supportive of its potential in vivo role in axon localization, reporters for both NCA-1(UNC-2) and NCA-1(EGL-19) chimeric channels failed to localize to axons in *C. elegans* neurons (Figure S7D).

An obvious caveat of this observation is that the misfolding and/or mistrafficking of chimeric channels do not necessarily involve the NLF-1 interaction. Intriguingly, the S5/P loop/S6 motif of the mammalian Kv1.1 channel has been shown by chimeric analysis to play a dominant role in its ER export and trafficking (Manganas et al., 2001). The S5/P loop/S6 segments of the ion transport motifs I and IV were shown to confer the gating specificity by distinct β_1 subunits for the different classes of Na_V channels (Makita et al., 1996). Collectively, these studies provide leads for future dissection of molecular mechanisms through which NLFs affect the Na^+ leak channel.

The topology of NLF-1 and mNLF-1 resembles that of a large protein family termed tail-anchored (TA) proteins, which contain

a single transmembrane domain within 40 residues of the C terminus and lack known N-terminal signal sequences (Borgese and Fasana, 2011). Some TA proteins are targeted to the ER (Wattenberg and Lithgow, 2001), and are proposed to function in protein trafficking (Shao and Hegde, 2011). Our results indicate a potential substrate specificity of TA proteins in membrane protein trafficking.

nlf-1 Animals Exhibit Slightly Less Severe Locomotion Defects Than *nca(lf)*

As fainters, *nlf-1* null mutants exhibit a slightly, but consistently, less severe degree of locomotion deficit than *nca(lf)*. Several possibilities could account for this subtle difference in phenotype severity. The expression patterns of translational reporters for NCA-1, NCA-2, and NLF-1 overlap extensively, but not entirely, in the *C. elegans* nervous system. A most noticeable difference is that our functional *nlf-1::GFP* reporter does not exhibit obvious expression in the GABAergic motor neurons (Figure S2H), raising a possibility that NLF-1 partakes NCA channel trafficking in most, but not all neurons. Another possibility is that a small fraction of the NCA channels could remain localized and functional in the absence of NLF-1. We favor the second possibility because expressing either NLF-1 or NCA-1 in the GABAergic motor neurons did not result in any noticeable improvement in the locomotion deficit in *nlf-1* or *nca(lf)* mutants (data not shown). Moreover, this small behavioral difference coincided with a subtle, yet also consistent, reduction in Na^+-dependent change in background leak current (ΔI; Figure 4C) and RMP (ΔV; Figure 4F) in the AVA premotor interneurons in *nlf-1* when compared to that in *nca(lf)* mutants.

The Na^+ Leak Channel Constitutes a Conserved Mechanism for Neuronal Excitability

We provide the first direct, physiological evidence for the NCA channel's role in maintaining neuronal RMP. Thus, in both the nonspiking *C. elegans* and spiking vertebrate neurons, this Na^+ leak channel constitutes a conserved mechanism that modulates neuronal excitability. Despite a modest sequence homology between NLF-1 and mNLF-1, and the differences in neuronal properties between vertebrate and *C. elegans* interneurons, mNLF-1 fully substitutes for NLF-1 when expressed in *C. elegans*. mNLF-1 exhibits enriched, broad expression in the mouse brain (http://mouse.brain-map.org). shRNA-mediated knockdown of mNLF-1 effectively, albeit partially reduces the Na^+ leak currents in primary cortical neuron cultures. Thus, while mNLF-1's physiological function awaits further investigation, our current studies imply its role in the folding/trafficking of the NALCN Na^+ leak channel. The ability of mNLF-1 to substitute NLF-1 in the *C. elegans* nervous system further highlights the conservation of machineries that modulate membrane physiology.

Removing extracellular Na^+ leads to a further hyperpolarization of RMP in both *nca(lf)* and *nlf-1* mutants, indicating the presence of additional Na^+ channels in modulating neuronal excitability. As the *C. elegans* genome does not encode voltage-gated Na^+ channels, machineries that carry out the remaining Na^+ conductance remain to be identified.

The Involvement of the NCA/NALCN Na^+ Leak Channel in Rhythmic Activity

How the Na^+ leak channel affects intact neural circuit activity remains to be explored. Intriguingly, *nalcn*$^{-/-}$ mice cannot generate respiratory rhythm (Lu et al., 2007); *na* flies fail to exhibit motor patterns associated with circadian cycles (Lear et al., 2005; Nash et al., 2002; Zhang et al., 2010); the knockdown of a snail NALCN homolog compromises respiratory function (Lu and Feng, 2011); the loss of NCA leads to disrupted rhythmicity in *C. elegans* locomotion (Pierce-Shimomura et al., 2008; this study). Collectively, these phenotypes imply a requirement of this channel in neural networks generating rhythmic behaviors.

Despite a broad expression in the *C. elegans* motor circuit, NLF-1 activity in motor neurons was neither necessary, nor sufficient to restore the continuity of locomotion. On the other hand, NLF-1 expression in premotor interneurons alone was sufficient to restore the rhythmicity of movements. These results indicate that a reduced premotor interneuron network activity, instead of a motor neuron dysfunction, is the primary cause of the frequent halting exhibited by fainters. This is consistent with the observation that the severity of fainting is modified by sensory inputs such as food deprivation (unpublished results).

How the *C. elegans* motor circuit initiates and maintains rhythmic locomotion remains a mystery. Fainters provide a genetic tool to pinpoint the minimal neural networks most critical for rhythm generation. The fact that NLF-1 expression is required in all premotor interneurons to fully prevent halting during locomotion suggests that the premotor interneuron network is necessary for sustained, rhythmic *C. elegans* movements, and the NCA/NLF-1-mediated sodium leak is a critical regulator of the premotor interneuron network activity.

Despite its recent discovery, this Na^+ leak channel has been implicated in additional, diverse biological functions (Ren, 2011), including volatile anesthetics sensitivity (Humphrey et al., 2007; Morgan et al., 1990), insulin secretion (Swayne et al., 2009), systemic osmoregulation (Sinke et al., 2011), and recently, a susceptibility to autism (Iossifov et al., 2012). Investigating NLF-1/mNLF-1 will provide further physiological and mechanistic insights into these potential roles.

EXPERIMENTAL PROCEDURES

NLF-1 and mNLF-1 Cloning

hp428 was mapped between *egl-17* and *unc-1*. A fosmid WRM0625aG07 rescued the fainter phenotype exhibited by *hp428* and reverted *nca(gf);hp428* to *nca(gf)*-like coilers. From WRM0625aG07, a 6.5 kb fragment containing a single open reading frame F55A4.2 fully rescued the fainter phenotype of *nlf-1(hp428)*. A G-to-A mutation at the first intron/second exon junction of F55A4.2 was identified by sequencing. A full-length *nlf-1* cDNA was generated by RT-PCR from *C. elegans* RNA, and the sequence was determined by sequencing (Supplemental Information). The cDNA sequence has been deposited to NCBI.

nlf-1(lf) mutants were crossed to TY2138 *meDf6;yDp15*, which carries a large deletion including the *nlf-1* locus. The locomotion of *nlf-1(hp428)* and *nlf-1(tm3631)* was undistinguishable from that of *nlf-1(hp428)/meDf6* and *nlf-1(tm3631)/meDf6* heterozygous animals, respectively; *hp428* and *tm3631* thus represent genetic null alleles for NLF-1.

Locomotion Analyses

Animals (12–18 hr post-L4 stage) were transferred to a 100 mm Nematode Growth Medium (NGM) plate seeded with a thin layer of OP50 12–14 hr before. One minute after the transfer, a two-minute movie of the crawling animal was recorded using a digital camera installed on a Leica MS5 dissecting microscope. Spontaneous movements exhibited by *C. elegans* were analyzed using an automated tracking program (Kawano et al., 2011).

For index of overall idle/active state, images were captured at 10× magnification and sampled at 1 fps. The center point of the animal is tracked to calculate its movement. A centroid change less than 1 pixel per second is defined as pausing. The percentage of total frames exhibiting motion versus pausing was calculated from the pooled image frames of multiple animals ($n > 10$) of each genotype.

For body bending curvature change overtime, young adult *C. elegans* was recorded at 40× magnification. Midline of the animal was extracted and divided into 37 equally spaced points from head to tail, and the curvature defined by adjacent points was tracked overtime. An anterior curvature (between point 8 and 9) was either pooled to be examined for distribution of the extent of body bending (Figure 1B), or to be plotted over time (Figure 3A) to quantify the mean frequency of bending cycles (Figure 1C).

Calcium Imaging

Premotor interneuron calcium imaging in moving *C. elegans* was performed using the *hpIs190* cameleon reporter as previously described (Kawano et al., 2011). AVA and AVE were coimaged as a single ROI as previously described. Periods of backward movements in each recording were isolated; differences of the YFP/CFP ratio between the base and the peak of the transient during each period were normalized against the baseline.

C. elegans Electrophysiology

Membrane potentials of AVA were recorded in whole-cell configuration at 20°C–22°C in a *C. elegans* interneuron preparation (Kawano et al., 2011) (modified from Brockie et al., 2001; Gao and Zhen, 2011; Richmond and Jorgensen, 1999). The pipette solution contained (in mM): K-Gluconate 115; KCl 25; $CaCl_2$ 0.1; $MgCl_2$ 5; BAPTA 1; HEPES 10; Na_2ATP 5; Na_2GTP 0.5; cAMP 0.5; cGMP 0.5, pH 7.2 with KOH, ~320 mOsm. cGMP and cAMP were included mainly to increase the longevity of the preparation (Brockie et al., 2001; Gao and Zhen, 2011); no significant difference of the steady state leak current was observed when they were removed from the pipette solutions (data not shown). The bath solution consisted of (in mM): NaCl 150; KCl 5; $CaCl_2$ 5; $MgCl_2$ 1; glucose 10; sucrose 5; HEPES 15, pH 7.3 with NaOH, ~330 mOsm. For zero and 15 Na^+ solution, extracellular Na^+ ($[Na^+]_o$) was replaced with N-methyl-D-glucamine ($NMDG^+$) or $Tris^+$. RMP was recorded at 0 pA. Healthy preparations were selected based on following criteria: whole-cell capacitance (1–2.2 pF), steady state leak current (−40 to 0 pA at −60 mV) and RMP (−40 to −15 mV, at 150 mM Na^+). For leak current change upon low Na^+ stimulation, recordings that recovered >70% leak current upon 150 mM Na^+ wash back were included for data analyses.

C. elegans Immunocytochemistry and Biochemistry

To generate antibodies against NLF-1, a mixture of bacterially expressed NLF-1 antigens (aa57–190, aa155–312, and aa265–400) was injected in a rabbit (Covance). NLF-1 antibodies were affinity purified against mixed antigens from the crude rabbit serum.

For immunocytochemistry, animals were fixed in 2% paraformaldehyde for 2h and stained as described (Yeh et al., 2008). For animals expressing NLF-1::GFP alone or with RFP-tagged ER/Golgi markers, antibodies against GFP (Invitrogen) and RFP (Chromoteck) were used at 1:100 and 1:50 dilutions, respectively. For staining animals coexpressing NLF-1 and mCherry tagged ER markers, antibodies against NLF-1 and RFP were used at 1:50 dilutions. Images of stained animals were acquired on a Nikon Eclipse 90i confocal microscope.

For *C. elegans* biochemistry, protein extracts were prepared as previously described (Gendrel et al., 2009). Briefly, 2 ml mixed stage *C. elegans* pellets were snap-frozen in liquid nitrogen, ground into powders and thawed in two volumes of ice-cold homogenization buffer (50 mM HEPES [pH 7.7], 50 mM KCl, 2 mM $MgCl_2$, 250 mM sucrose, 1 mM EDTA pH 8, 2 mM PMSF and mini Protease inhibitor cocktail [Roche, two tablets per 50 ml]). The suspension was further homogenized by sonication and centrifuged at 6,000 × g for 15 min at 4°C to remove debris. The supernatant was incubated with 10× glycoprotein denaturing buffer (NEB) at 75°C for 15 min, and the denatured protein lysates were incubated with either endoglycosidase H (EndoH, Roche) or PNGase F (NEB) for 3 hr at 37°C. The reaction was terminated by incubation at 75°C for 10 min in 1× SDS sample buffer. For western blot analyses, NLF-1::RFP was detected with anti-RFP antibody (Chromoteck) at 1:1,000.

Immunocytochemistry and Biochemistry in Mammalian Cell Cultures

COS-7 and HEK293 cells were maintained in DMEM supplemented with 10% FBS, 200 U/ml penicillin and 200 μg/ml streptomycin at 37°C with 5% CO_2. Cells were plated on polyethyleneimine (PEI)-coated culture dishes or coverslips. Eighteen to twenty-four hours after plating, cells were transfected with 4 μg, 9 μg, or 30 μg of DNA (for 35 mm, 60 mm, and 150 mm dishes) using Lipofectamine 2000 (Invitrogen). For immunoprecipitation, cells were scraped and lysed in 0.8 ml lysis buffer (1% NP-40, 150 mM NaCl, 10% glycerol, 50 mM Tris [pH 7.5], protease inhibitor cocktail). Lysates were cleared at 540,000 × g for 15 min at 4°C. To pull down FLAG::NALCN, supernatants were incubated with anti-FLAG antibodies (Sigma) for 2 hr, followed by Protein G Sepharose beads (GE Healthcare) for 1 hr. To immunoprecipitate GFP::mUNC-80, mNLF-1::GFP, or mNLF-1::RFP, supernatants were incubated with anti-GFP or anti-RFP beads (Chromotek) for 2 hr. Beads were washes five times with the lysis buffer and eluded by the SDS-PAGE buffer. For glycosidase treatment, cell pellets were resuspended in denaturing buffer, and incubated at 90°C for 10 min, followed by Endo H (Roche) or PNGaseF (NEB) treatment at 37°C for 3 hr.

To compare NALCN level in the presence or absence of mNLF-1, FLAG-NALCN, and EGFP was coexpressed with a CMV promoter, and mNLF-1::mCherry was expressed by an EF1 promoter. For mock control, an equal amount of the empty vector (for mNLF-1 expression) was cotransfected in COS-7 cells; α-tubulin served as the loading controls, and EGFP served as the NALCN expression internal control.

For immunostaining, cells cultured on PEI- or poly-L-lysine-coated coverslips were fixed with 4% paraformaldehyde and 0.1% Triton X-100 and stained with mouse anti-GM130 (1/500; BD Biosciences), Calnexin (1/100; BD Biosciences), WGA-AlexaFluor 488 (Invitrogen) and anti-Na^+/K^+ ATPase (a gift from Dr. Takahashi) primary antibodies, and Alexa 546 goat anti-mouse secondary antibodies (Invitrogen).

shRNA Knockdown of mNLF-1 and Electrophysiology in Mouse Cortical Neurons

All experiments were approved by the local committee on animal care and conformed to the national guidelines (CCAC; http://www.ccac.ca). Cortical neurons were dissociated from E14 C57BL/6 mice, and plated on 35 mm dishes layered with poly-D-lysine coated slides at a density of 5×10^5 cells/cm^2. Starting medium consisted of high glucose DMEM supplemented with 40% FBS. Cells were maintained at 37°C and 5% CO_2 for 2–6 hr, after which the media was changed to Neurobasal A (GIBCO) supplemented with B-27, glutamine, and sodium pyruvate. Cells were transfected with 2 μg of target shRNA (pJH3044) or scrambled shRNA (pJH3045) constructs using Lipofectamine 2000 at DIV6. Recordings were performed at DIV8.

Leak currents of the primary mouse cortical neurons were recorded in whole-cell configuration at 20°C–22°C, modified from Lu et al. (2007) and Raman et al. (2000). The pipette solution contained (in mM): K-Gluconate 115; KCl 25; $CaCl_2$ 0.1; $MgCl_2$ 5; BAPTA 1; HEPES 10; Na_2ATP 5; Na_2GTP 0.5; cAMP 0.5; cGMP 0.5, pH 7.2 with KOH, ~320 mOsm. The bath solution consisted of (in mM): NaCl 150; KCl 5; $CaCl_2$ 2; $MgCl_2$ 4; D-glucose 10; sucrose 5; HEPES 10, TEACl 1, CsCl 2, pH 7.4 with Tris-OH, ~320 mOsm. For 15mM Na^+ solution, $[Na^+]_o$ was supplemented with $Tris^+$. Cells with steady state leak currents −40 to 5 pA at −85 mV were analyzed.

To test the efficacy of mNLF-1 knockdown, 2 μg pJH3096 (mNLF-1::RFP) were cotransfected with 2 μg pJH3044 or pJH3045. Western blot analysis was performed with antibodies against RFP (Chromoteck) at 1:1,000.

Acute Rescue of *nlf-1* Mutants

nlf-1(hp428) animals carrying an integrated NCA-1::GFP (or NCA-2::GFP) reporter, and an extrachromosomal array expressing NLF-1 cDNA under *Phsp-16.2* (pPD49.78) were maintained at 15°C. L4 stage animals were transferred to 32°C for 3h, and maintained at 25°C overnight prior to confocal imaging.

Additional Methods

Information on strains and constructs, quantitative epifluorescent and confocal microscopy, and membrane yeast two-hybrid (MYTH) assays are provided in Supplemental Information.

ACCESSION NUMBERS

The full length *nlf-1* cDNA sequence has been deposited to NCBI (accession number KC514050).

SUPPLEMENTAL INFORMATION

Supplemental Information includes seven figures, one movie, and Supplemental Experimental Procedures and can be found with this article online at http://dx.doi.org/10.1016/j.neuron.2013.01.018.

ACKNOWLEDGMENTS

We thank the *Caenorhabditis Genetics Center* and National Bioresource Project for strains, Cori Bargmann for ER and Golgi markers and UNC-2 cDNA, Mario de Bono for EGL-19::GFP strains, Mike Nonet for UNC-10 antibodies, and Dejian Ren for NALCN and mUNC-80 cDNAs. We thank Sharon Ng, Hang Li, Taizo Kawano, Zhi Xu, and Dan Zu for technical and programming support, Victoria Wong and Ria Lim for advice on MYTH and shRNA knockdown, respectively, and H. McNeill and S. Cordes for access to equipments and reagents. S.M.A. was supported by a National Sciences and Engineering Research Council postgraduate fellowship. This work was supported by the Canadian Institute of Health Research grants (MOP74530 and MOP123250) to M.Z. I.S. received Canadian Institute of Health Research grants.

Accepted: January 15, 2013
Published: March 20, 2013

REFERENCES

Altier, C., Garcia-Caballero, A., Simms, B., You, H., Chen, L., Walcher, J., Tedford, H.W., Hermosilla, T., and Zamponi, G.W. (2011). The Cavβ subunit prevents RFP2-mediated ubiquitination and proteasomal degradation of L-type channels. Nat. Neurosci. *14*, 173–180.

Arellano-Carbajal, F., Briseño-Roa, L., Couto, A., Cheung, B.H., Labouesse, M., and de Bono, M. (2011). Macoilin, a conserved nervous system-specific ER membrane protein that regulates neuronal excitability. PLoS Genet. *7*, e1001341.

Basham, S.E., and Rose, L.S. (2001). The *Caenorhabditis elegans* polarity gene ooc-5 encodes a Torsin-related protein of the AAA ATPase superfamily. Development *128*, 4645–4656.

Borgese, N., and Fasana, E. (2011). Targeting pathways of C-tail-anchored proteins. Biochim. Biophys. Acta *1808*, 937–946.

Brockie, P.J., Mellem, J.E., Hills, T., Madsen, D.M., and Maricq, A.V. (2001). The *C. elegans* glutamate receptor subunit NMR-1 is required for slow NMDA-activated currents that regulate reversal frequency during locomotion. Neuron *31*, 617–630.

Catterall, W.A. (2000a). From ionic currents to molecular mechanisms: the structure and function of voltage-gated sodium channels. Neuron *26*, 13–25.

Catterall, W.A. (2000b). Structure and regulation of voltage-gated Ca^{2+} channels. Annu. Rev. Cell Dev. Biol. *16*, 521–555.

Crill, W.E. (1996). Persistent sodium current in mammalian central neurons. Annu. Rev. Physiol. *58*, 349–362.

Denecke, J., De Rycke, R., and Botterman, J. (1992). Plant and mammalian sorting signals for protein retention in the endoplasmic reticulum contain a conserved epitope. EMBO J. *11*, 2345–2355.

Deribe, Y.L., Wild, P., Chandrashaker, A., Curak, J., Schmidt, M.H., Kalaidzidis, Y., Milutinovic, N., Kratchmarova, I., Buerkle, L., Fetchko, M.J., et al. (2009). Regulation of epidermal growth factor receptor trafficking by lysine deacetylase HDAC6. Sci. Signal. *2*, ra84.

Deutsch, C. (2003). The birth of a channel. Neuron *40*, 265–276.

Gao, S., and Zhen, M. (2011). Action potentials drive body wall muscle contractions in *Caenorhabditis elegans*. Proc. Natl. Acad. Sci. USA *108*, 2557–2562.

Gendrel, M., Rapti, G., Richmond, J.E., and Bessereau, J.L. (2009). A secreted complement-control-related protein ensures acetylcholine receptor clustering. Nature *461*, 992–996.

Gisler, S.M., Kittanakom, S., Fuster, D., Wong, V., Bertic, M., Radanovic, T., Hall, R.A., Murer, H., Biber, J., Markovich, D., et al. (2008). Monitoring protein-protein interactions between the mammalian integral membrane transporters and PDZ-interacting partners using a modified split-ubiquitin membrane yeast two-hybrid system. Mol. Cell. Proteomics *7*, 1362–1377.

Gong, Q., Keeney, D.R., Molinari, M., and Zhou, Z. (2005). Degradation of trafficking-defective long QT syndrome type II mutant channels by the ubiquitin-proteasome pathway. J. Biol. Chem. *280*, 19419–19425.

Grunwald, M.E., and Kaplan, J.M. (2003). Mutations in the ligand-binding and pore domains control exit of glutamate receptors from the endoplasmic reticulum in *C. elegans*. Neuropharmacology *45*, 768–776.

Halevi, S., McKay, J., Palfreyman, M., Yassin, L., Eshel, M., Jorgensen, E., and Treinin, M. (2002). The *C. elegans* ric-3 gene is required for maturation of nicotinic acetylcholine receptors. EMBO J. *21*, 1012–1020.

Helenius, A., and Aebi, M. (2001). Intracellular functions of N-linked glycans. Science *291*, 2364–2369.

Hille, B. (2001). Ion Channels of Excitable Membranes, Third Edition (Sunderland, MA: Sinauer).

Hodgkin, A.L., and Katz, B. (1949). The effect of sodium ions on the electrical activity of giant axon of the squid. J. Physiol. *108*, 37–77.

Humphrey, J.A., Hamming, K.S., Thacker, C.M., Scott, R.L., Sedensky, M.M., Snutch, T.P., Morgan, P.G., and Nash, H.A. (2007). A putative cation channel and its novel regulator: cross-species conservation of effects on general anesthesia. Curr. Biol. *17*, 624–629.

Iossifov, I., Ronemus, M., Levy, D., Wang, Z., Hakker, I., Rosenbaum, J., Yamrom, B., Lee, Y.H., Narzisi, G., Leotta, A., et al. (2012). De novo gene disruptions in children on the autistic spectrum. Neuron *74*, 285–299.

Johnsson, N., and Varshavsky, A. (1994). Split ubiquitin as a sensor of protein interactions in vivo. Proc. Natl. Acad. Sci. USA *91*, 10340–10344.

Jospin, M., Watanabe, S., Joshi, D., Young, S., Hamming, K., Thacker, C., Snutch, T.P., Jorgensen, E.M., and Schuske, K. (2007). UNC-80 and the NCA ion channels contribute to endocytosis defects in synaptojanin mutants. Curr. Biol. *17*, 1595–1600.

Kawano, T., Po, M.D., Gao, S., Leung, G., Ryu, W.S., and Zhen, M. (2011). An imbalancing act: gap junctions reduce the backward motor circuit activity to bias *C. elegans* for forward locomotion. Neuron *72*, 572–586.

Lansdell, S.J., Gee, V.J., Harkness, P.C., Doward, A.I., Baker, E.R., Gibb, A.J., and Millar, N.S. (2005). RIC-3 enhances functional expression of multiple nicotinic acetylcholine receptor subtypes in mammalian cells. Mol. Pharmacol. *68*, 1431–1438.

Lear, B.C., Lin, J.M., Keath, J.R., McGill, J.J., Raman, I.M., and Allada, R. (2005). The ion channel narrow abdomen is critical for neural output of the *Drosophila* circadian pacemaker. Neuron *48*, 965–976.

Lee, R.Y., Lobel, L., Hengartner, M., Horvitz, H.R., and Avery, L. (1997). Mutations in the alpha1 subunit of an L-type voltage-activated Ca2+ channel cause myotonia in *Caenorhabditis elegans*. EMBO J. *16*, 6066–6076.

Lu, T.Z., and Feng, Z.P. (2011). A sodium leak current regulates pacemaker activity of adult central pattern generator neurons in *Lymnaea stagnalis*. PLoS ONE *6*, e18745.

Lu, B., Su, Y., Das, S., Liu, J., Xia, J., and Ren, D. (2007). The neuronal channel NALCN contributes resting sodium permeability and is required for normal respiratory rhythm. Cell *129*, 371–383.

Lu, B., Su, Y., Das, S., Wang, H., Wang, Y., Liu, J., and Ren, D. (2009). Peptide neurotransmitters activate a cation channel complex of NALCN and UNC-80. Nature *457*, 741–744.

Lu, B., Zhang, Q., Wang, H., Wang, Y., Nakayama, M., and Ren, D. (2010). Extracellular calcium controls background current and neuronal excitability via an UNC79-UNC80-NALCN cation channel complex. Neuron *68*, 488–499.

Makita, N., Bennett, P.B., and George, A.L., Jr. (1996). Molecular determinants of beta 1 subunit-induced gating modulation in voltage-dependent Na^+ channels. J. Neurosci. *16*, 7117–7127.

Manganas, L.N., Wang, Q., Scannevin, R.H., Antonucci, D.E., Rhodes, K.J., and Trimmer, J.S. (2001). Identification of a trafficking determinant localized to the Kv1 potassium channel pore. Proc. Natl. Acad. Sci. USA *98*, 14055–14059.

Morgan, P.G., Sedensky, M., and Meneely, P.M. (1990). Multiple sites of action of volatile anesthetics in *Caenorhabditis elegans*. Proc. Natl. Acad. Sci. USA *87*, 2965–2969.

Nash, H.A., Scott, R.L., Lear, B.C., and Allada, R. (2002). An unusual cation channel mediates photic control of locomotion in *Drosophila*. Curr. Biol. *12*, 2152–2158.

Nicholls, J.G., Martin, R.A., and Wallace, B.G. (2001). From Neuron to Brain, Fourth Edition (Sunderland, MA: Sinauer).

Palty, R., Raveh, A., Kaminsky, I., Meller, R., and Reuveny, E. (2012). SARAF inactivates the store operated calcium entry machinery to prevent excess calcium refilling. Cell *149*, 425–438.

Pierce-Shimomura, J.T., Chen, B.L., Mun, J.J., Ho, R., Sarkis, R., and McIntire, S.L. (2008). Genetic analysis of crawling and swimming locomotory patterns in *C. elegans*. Proc. Natl. Acad. Sci. USA *105*, 20982–20987.

Raman, I.M., Gustafson, A.E., and Padgett, D. (2000). Ionic currents and spontaneous firing in neurons isolated from the cerebellar nuclei. J. Neurosci. *20*, 9004–9016.

Ren, D. (2011). Sodium leak channels in neuronal excitability and rhythmic behaviors. Neuron *72*, 899–911.

Richmond, J.E., and Jorgensen, E.M. (1999). One GABA and two acetylcholine receptors function at the *C. elegans* neuromuscular junction. Nat. Neurosci. *2*, 791–797.

Saheki, Y., and Bargmann, C.I. (2009). Presynaptic CaV2 calcium channel traffic requires CALF-1 and the alpha(2)delta subunit UNC-36. Nat. Neurosci. *12*, 1257–1265.

Semenza, J.C., Hardwick, K.G., Dean, N., and Pelham, H.R. (1990). ERD2, a yeast gene required for the receptor-mediated retrieval of luminal ER proteins from the secretory pathway. Cell *61*, 1349–1357.

Shao, S., and Hegde, R.S. (2011). Membrane protein insertion at the endoplasmic reticulum. Annu. Rev. Cell Dev. Biol. *27*, 25–56.

Simms, B.A., and Zamponi, G.W. (2012). Trafficking and stability of voltage-gated calcium channels. Cell. Mol. Life Sci. *69*, 843–856.

Sinke, A.P., Caputo, C., Tsaih, S.W., Yuan, R., Ren, D., Deen, P.M., and Korstanje, R. (2011). Genetic analysis of mouse strains with variable serum sodium concentrations identifies the Nalcn sodium channel as a novel player in osmoregulation. Physiol. Genomics *43*, 265–270.

Swayne, L.A., Mezghrani, A., Varrault, A., Chemin, J., Bertrand, G., Dalle, S., Bourinet, E., Lory, P., Miller, R.J., Nargeot, J., and Monteil, A. (2009). The NALCN ion channel is activated by M3 muscarinic receptors in a pancreatic beta-cell line. EMBO Rep. *10*, 873–880.

Waithe, D., Ferron, L., Page, K.M., Chaggar, K., and Dolphin, A.C. (2011). Beta-subunits promote the expression of $Ca_{(V)}2.2$ channels by reducing their proteasomal degradation. J. Biol. Chem. *286*, 9598–9611.

Wattenberg, B., and Lithgow, T. (2001). Targeting of C-terminal (tail)-anchored proteins: understanding how cytoplasmic activities are anchored to intracellular membranes. Traffic *2*, 66–71.

Yeh, E., Ng, S., Zhang, M., Bouhours, M., Wang, Y., Wang, M., Hung, W., Aoyagi, K., Melnik-Martinez, K., Li, M., et al. (2008). A putative cation channel, NCA-1, and a novel protein, UNC-80, transmit neuronal activity in *C. elegans*. PLoS Biol. *6*, e55.

Zhang, L., Chung, B.Y., Lear, B.C., Kilman, V.L., Liu, Y., Mahesh, G., Meissner, R.A., Hardin, P.E., and Allada, R. (2010). DN1(p) circadian neurons coordinate acute light and PDF inputs to produce robust daily behavior in *Drosophila*. Curr. Biol. *20*, 591–599.